FEBEX Stage2

UPC modelling report 2020

Alfonso Rodriguez-Dono

January 2020

FEBEX Stage2 ─ UPC modelling report 2020

1. Introduction

The present report contains the description of a model for the large-scale in situ heating test FEBEX (full-scale engineered barrier experiment). In this test, after five years of heating, one of the heaters was switched off and the experiment was partially dismantled, allowing the final state of the barrier to be observed directly. In this way, very valuable information on the state of the bentonite at the end of the test was obtained. The test has received attention during the initial (Gens et al., 1998) and intermediate stages (Alonso & Alcoverro, 2005). Moreover, Gens et al. (2009) discussed the thermal, hydraulic and mechanical observations in the bentonite barrier and in the host rock, paying special attention to the progress of hydration in the barrier, the effects of heating and vapour transport, and the development of swelling pressures in the barrier.

In the FEBEX experiment, heaters are emplaced in the axis of a tunnel excavated in granite to simulate the heat production of radioactive waste. The test is fully instrumented, and attention is focused on the thermo-hydro-mechanical (THM) behaviour of the near-field region constituted by the compacted bentonite barrier surrounding the heater and the immediately adjacent rock. Interpretation of the test is assisted by the performance of a coupled numerical analysis based on a formulation that incorporates the relevant THM phenomena. Further description of the FEBEX in situ test can be found in Gens et al. (2009).

The model of this test has been developed using CODE_BRIGHT (Olivella et al., 1994 and 1996), a Finite Element Method program that enables coupled thermo-hydro-mechanical analysis in geological media. This is a code version that incorporates customized pre- and post- process interfaces so that simulation models that use CODE_BRIGHT ─available from https://deca.upc.edu/en/projects/code_bright─ can be developed more easily. It allows easy modification of parameters, boundary conditions, excavation protocols, meshing and organization of calculation intervals. The reason is that it has been developed using the GiD interface (http://www.gidhome.com) that permits pre- and post- process of data in a user-friendly way.

The model for FEBEX presented in this report is based on the FEBEX Task 9 specifications document (Gens, 2017) and on the material properties of previous modelling efforts (Gens et al., 2009; Sanchez et al., 2012; Rodriguez-Dono et al., 2018).

Furthermore, Rodriguez-Dono et al. (2018) also developed a model of the well-known FEBEX experiment that was exploited in terms of the implementation of additional processes such as coupled flows and double structure models to investigate their impact of hydration and stress development.

Additional information on the full FEBEX project and its modelling is given in Huertas et al. (2006), Sanchez & Gens (2006), Tadikonda (2014), Bendito & Pintado (2016), Villar (2002), Villar et al. (2018) and Toprak et al. (2018).

Finally, the main objective of this report is to contribute to an enhancing understanding of the interplay between numerical modelling results and the observations of the in situ test. The comparison between modelling results and observations as well as the comparison between the results of the different codes used by different teams are a key tool to achieve this enhanced understanding.

2. UPC's FEBEX model

2.1. General features of the numerical analysis

The model developed analyses the **coupled thermo-hydro-mechanical** (**THM**) behaviour of the geological media using Code_Bright v9 and GiD 14. The geometry of the model has been taken from the FEBEX Task 9 specifications document (Gens, 2017) ─see Figure 1. In addition, in this figure, the location of the instrumented sections can be observed.

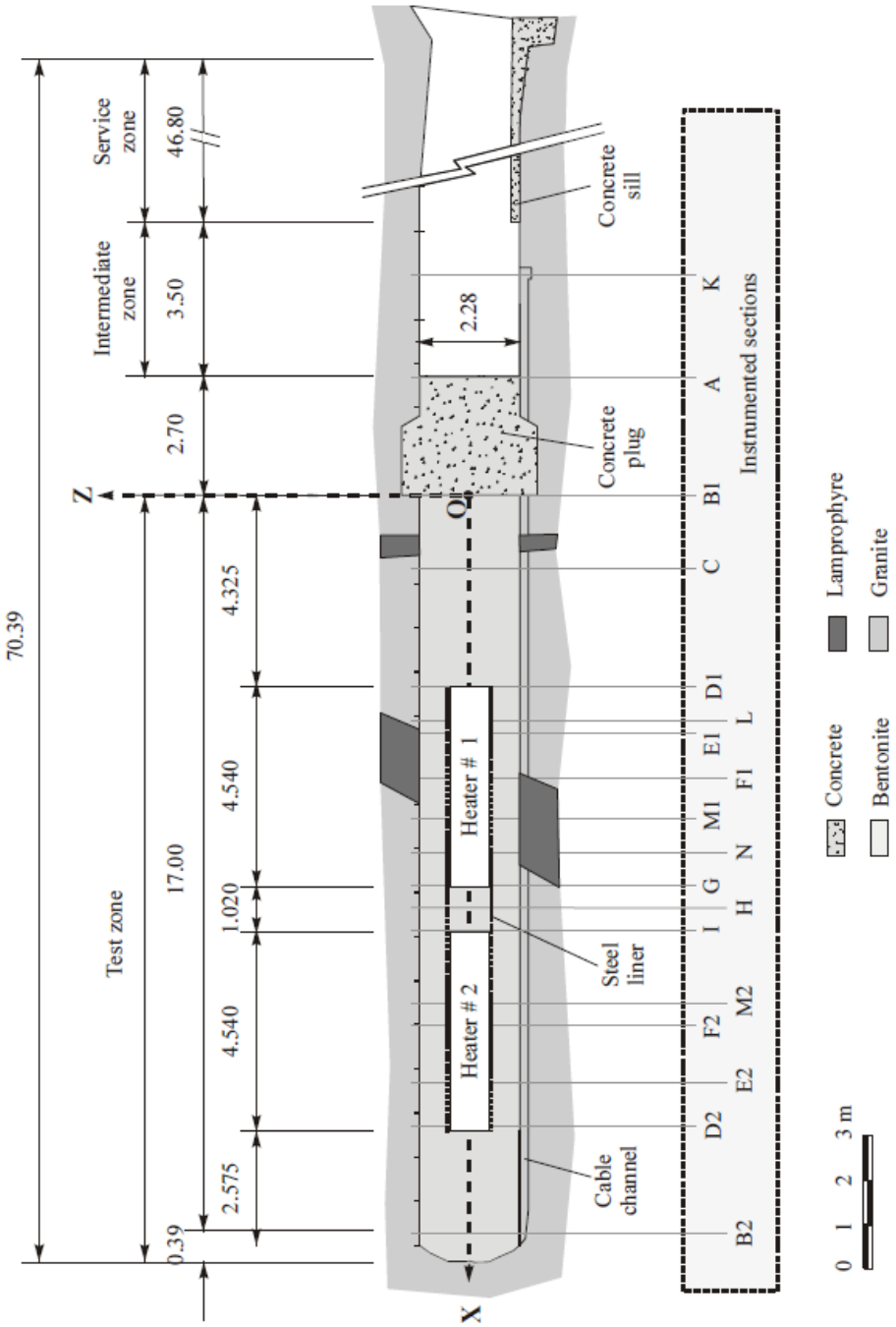

Figure 1. FEBEX in-situ experiment geometry (Gens, 2017).

Figure 2 shows the geometry and materials considered in this model. The host rock (granite), the bentonite buffer (divided in Bentonite and Bentonite2 to allow the partial dismantling of the bentonite buffer), the concrete plug and the canister (heaters #1 and #2) are the materials considered. After the first dismantling, the heater #1 is removed and partially replaced by a dummy. Each heater has a volume of 2.888 m^3. The model is two-dimensional, assuming **axisymmetry** along the tunnel axis. **The dimensions of the model are 30 m by 31.2 m**.

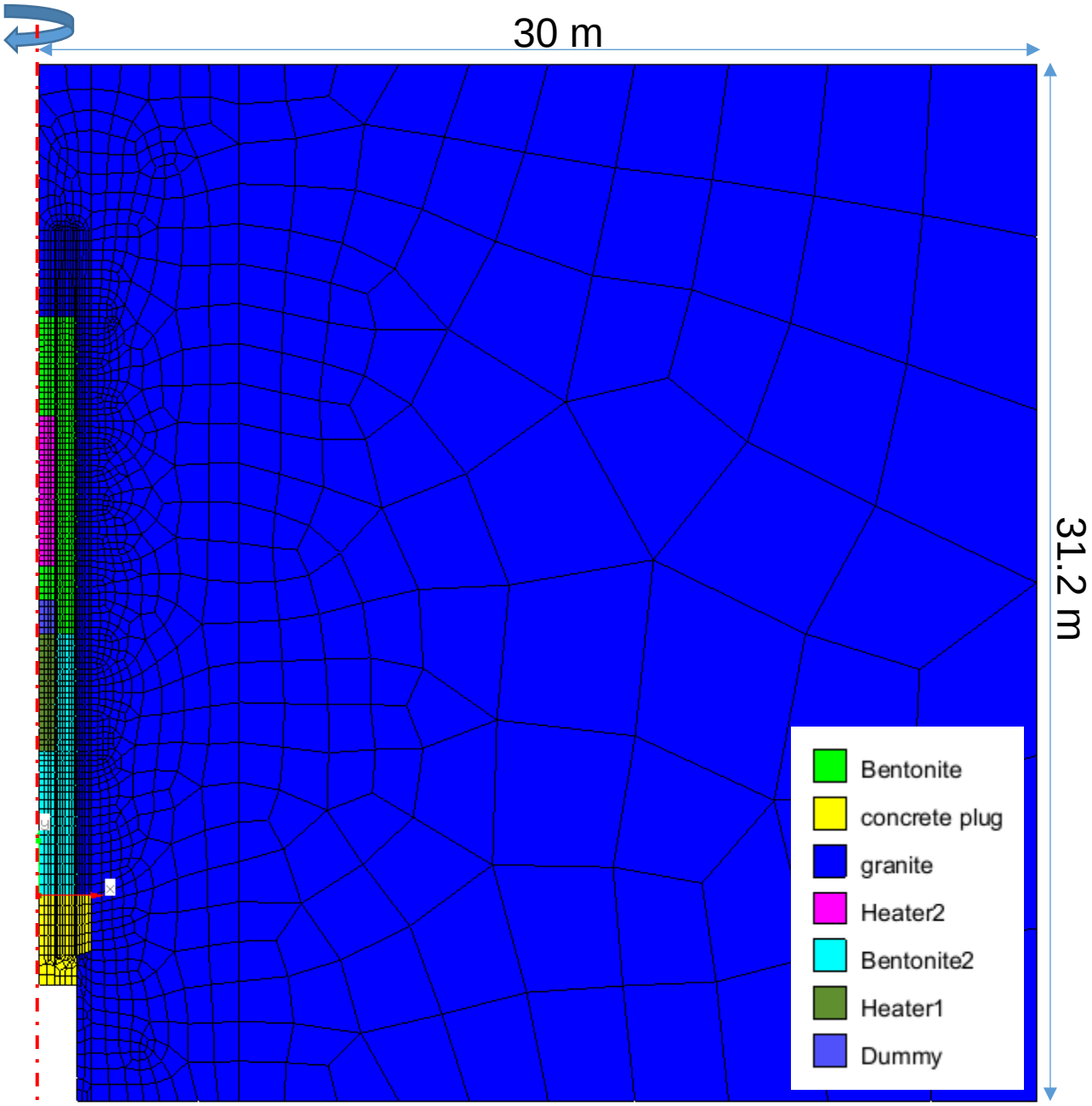

Figure 1. Model geometry, materials and mesh considered for UPC's FEBEX model.

The mesh of the model is composed of **3049 linear quadrilateral elements and 3139 nodes**. Unlike the model used in Gens et al. (2009), this model takes advantage of the unstructured mesh development for the discretization of the host rock. With an unstructured mesh, the model will have less elements in the host rock section and thus, it will run faster. However, the buffer is discretized with a structured mesh, as this is more adequate in the zone of interest to reduce numerical errors.

Across the bentonite barrier, there are 10 elements (Figure 2). The mesh is refined near the heater and near the granite, where the bigger gradients of temperature, pore water pressure, etc. are achieved. In fact, the second element –counting from the heater at r=0.45 m– starts at r=0.489 m and the penultimate element ends at r=1.101 m before reaching the granite at r=1.14 m. Therefore, it would be fair to say that those 10 elements are equivalent to around 17 same-sized elements across the bentonite buffer, at least in terms of the numerical precision.

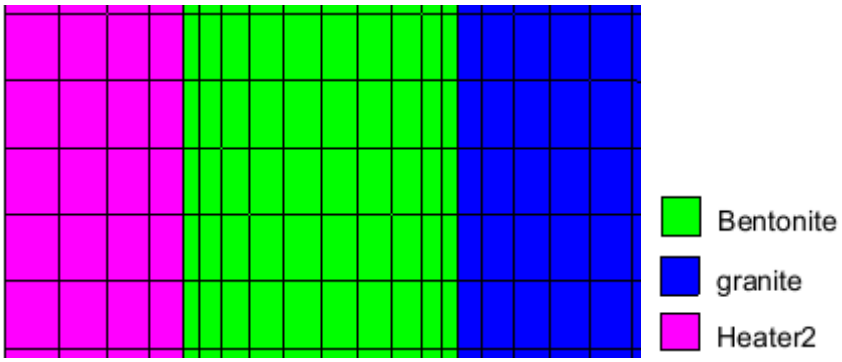

Figure 2. Close view of the elements across the bentonite barrier.

Table 1 shows the intervals considered in the analysis up to 6758 days, i.e. until the final dismantling of the test. Heaters switch on at day 0 and day 1968 would correspond to the end of the first dismantling.

In order to match the measured evolution of temperature during the experiment (see more details about this in Gens et al., 2009), the heat power was progressively modified (see table 1) until the 100ºC target temperature was reached.

Note that the design conditions of the experiment contemplate a maximum temperature of 100°C at the contact between the heater and bentonite (Villar, 2002; Huertas et al., 2006); since it is assumed that engineered clay barriers do not change their properties for temperatures below 100ºC.

From that point on, the temperature was prescribed at the value of 100ºC in both heaters. Later, one of the heaters was removed but the other continued heating until day 6630, in which heater #2 was switch off.

The initial and boundary conditions, as well as the mechanical, hydraulic and thermal parameters used in the model will be described in the sections below.

Table 1. Time intervals considered for the simulation up to 6758 days.

Stage number	Brief description	Start time (day)	Duration (day)	Prescribed heat flow on heaters $\left(\frac{J}{s\ m^3}\right)$	Prescribed temperature (C)
1	Excavation in granite rock	-200	65	0	12 (far rock)
2	Construction of bentonite, canisters and concrete plug	-135	135	0	12 (far rock)
3	Heaters switch on to 1200 W	0	20	415.5	12 (far rock)
4	Heaters to 2000 W	20	33	692.5	12 (far rock)
5	Heaters at 100°C	53	1774	0	12 (far rock) 100 (heaters)
6	Heater #1 switch off Heater #2 at 100°C	1827	39	0	12 (far rock) — (heater #1) 100 (heater #2)
7	Concrete plug demolition	1866	50	0	12 (far rock) 100 (heater #2)
8	First dismantling of bentonite and heater#1	1916	52	0	12 (far rock) 100 (heater #2)
9	Extended transition before final dismantling	1968	4662	0	12 (far rock) 100 (heater #2)
10	Heater #2 switch off	6630	128	0	12 (far rock) — (heater #2)

2.2. Initial and boundary conditions

2.2.1. Boundary conditions

A mechanical boundary condition restraining the normal displacements has been applied all along the external boundary for all time intervals (Figure 3). Also, after the demolition of the concrete plug (interval 7), the normal displacements to the now exposed bentonite have been fixed (Figure 4a). Similarly, the normal displacements of the exposed bentonite after the first dismantling have also been fixed (Figure 4b).

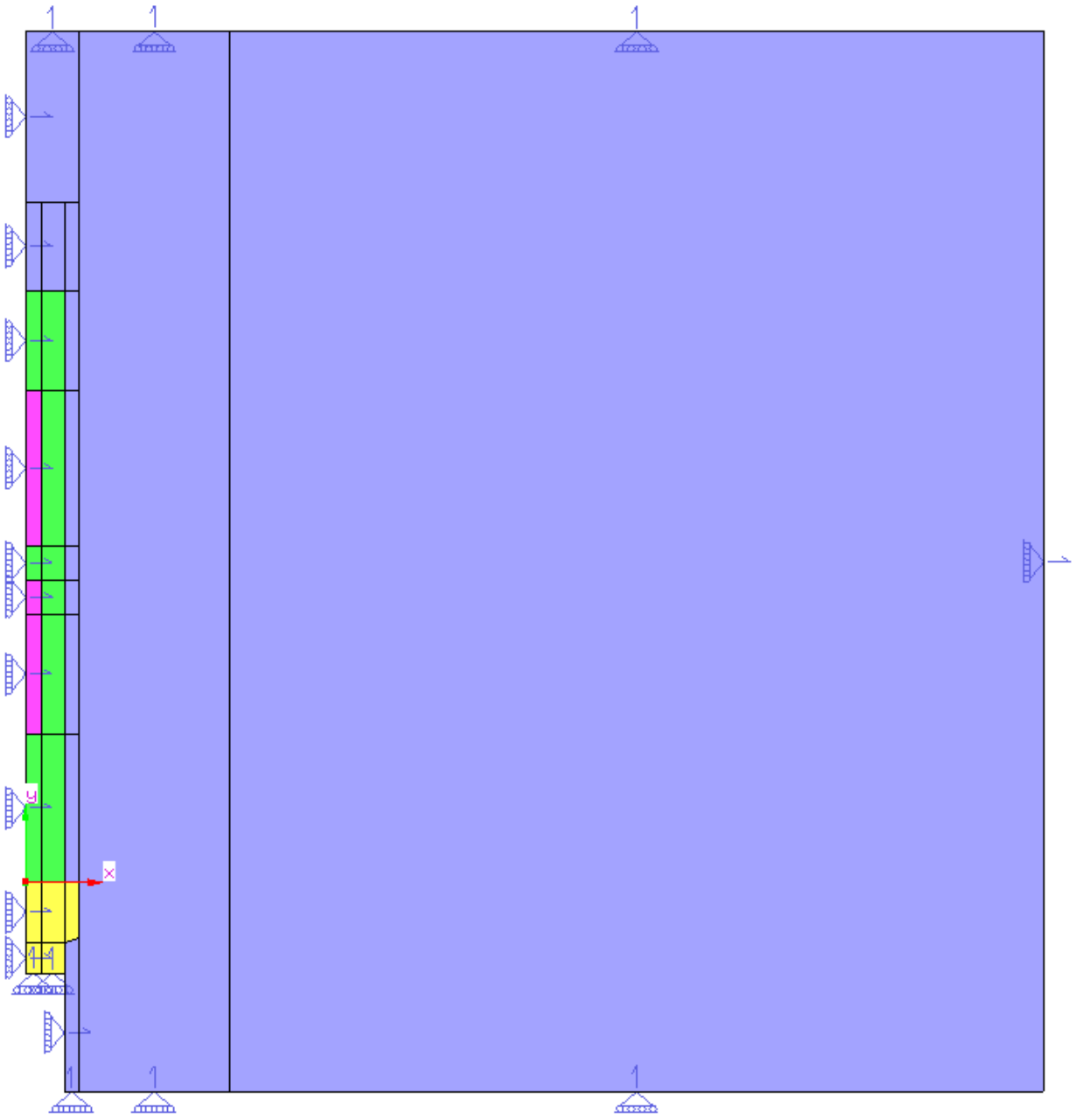

Figure 3. Mechanical boundary conditions at the beginning of the simulation.

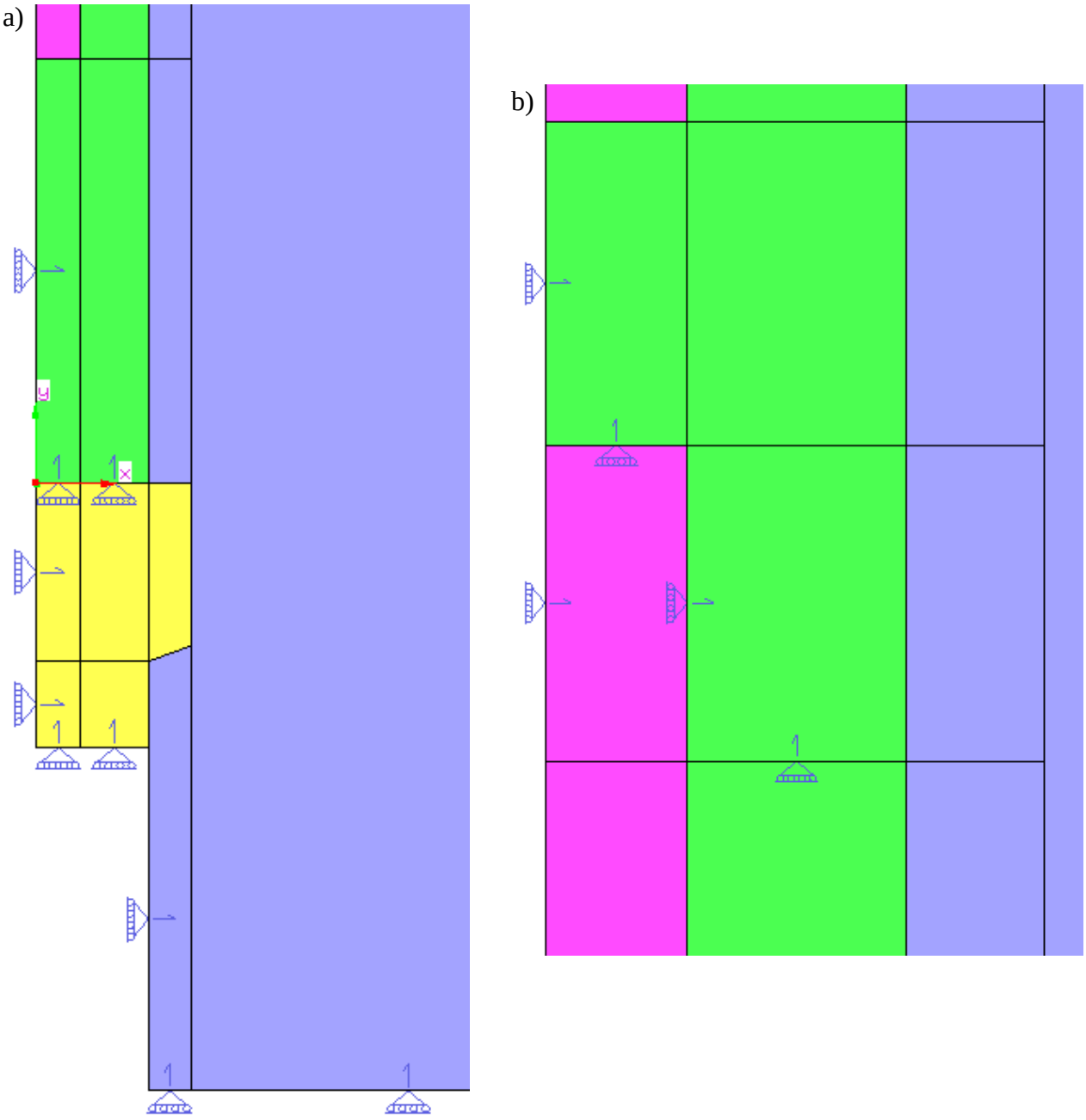

Figure 4. Mechanical boundary conditions (a) after the demolition of the concrete plug and (b) after the first dismantling.

In addition, a constant pore water pressure of 0.9 MPa is imposed on the external boundary, corresponding to the unaltered far host rock (granite). To simulate ventilation, a pore water pressure of -1 MPa has been set in the excavated tunnels before construction of the bentonite buffer (interval 1; Figure 5) or after dismantling. Moreover, a pore water pressure of -1 MPa has been set on the remaining unconstructed tunnel walls (in front of the concrete plug).

As indicated above (Table 1), during intervals 3 and 4 the power of the heaters is prescribed and therefore the temperature increases. The power is prescribed using the equivalent volumetric flow rate in both heaters to first 1200 W (interval 3) and then 2000 W (interval 4). Once the temperature reaches the target value on the surface canister (100 ºC), the boundary condition on the heater is changed from constant power to a constant temperature of 100 ºC (interval 5). Then, heater #1 is switched off at day 1827 (interval 6) and heater #2 is switched off at day 6630 (interval 10).

More information about boundary condition implementation in the Code_Bright User's Guide (2018), downloadable from the Code_Bright web page − deca.upc.edu/en/projects/code_bright).

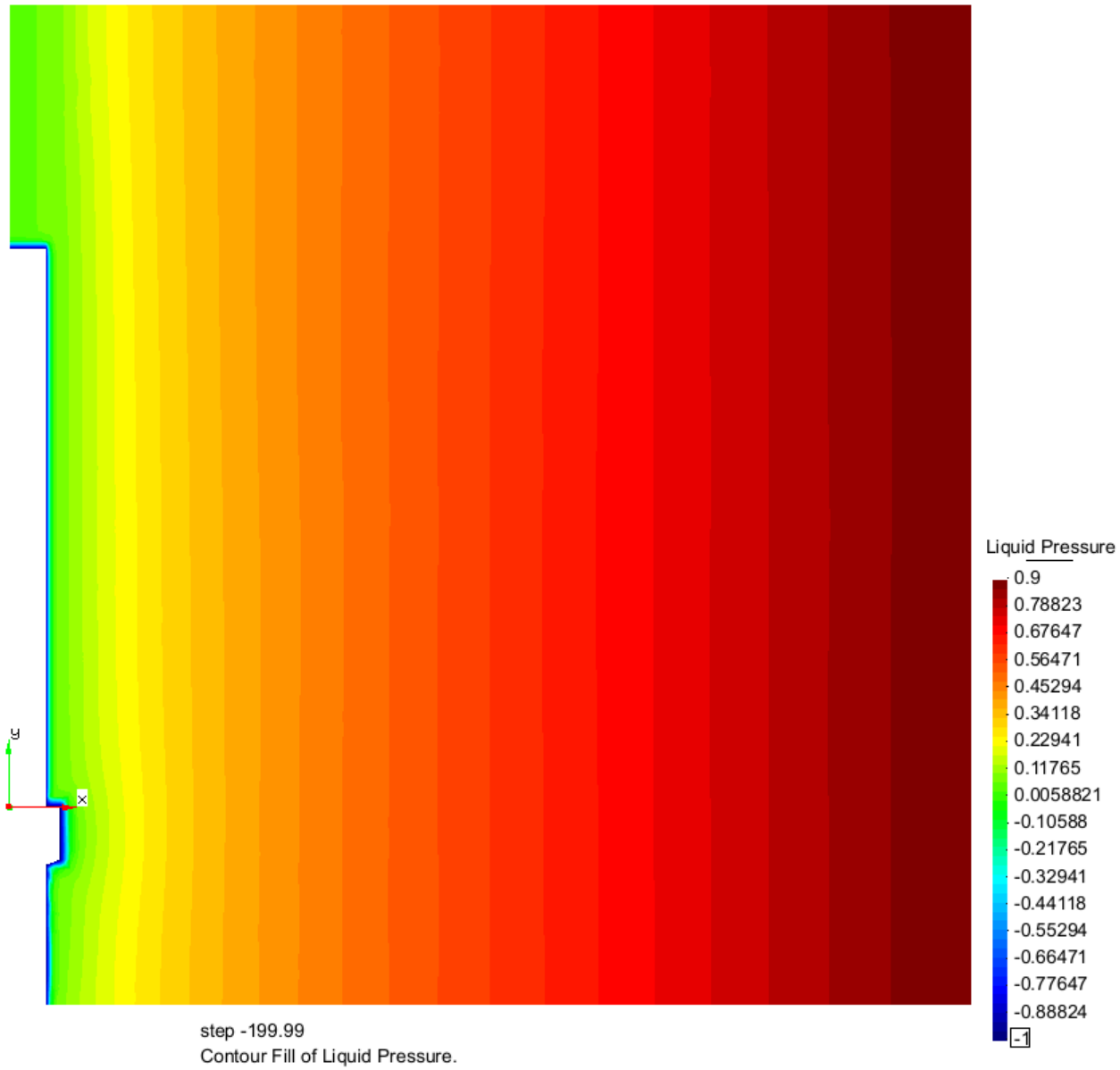

Figure 5. Pore water pressure at the beginning of the simulation (interval 1; time = -200 days).

2.2.2. Initial conditions

The initial stress has been set to -28 MPa in the granite and to -0.1 MPa in the rest of the materials (negative values correspond to compression). The initial pore water pressure in the rock follows a linear distribution from 0.9 MPa at 30 m from the tunnel axis until 0.1 MPa at 2.28 m from the tunnel axis (Figure 5). The initial temperature of all materials (including the rock) has been set to 12 ºC. Finally, an initial porosity of 0.1 has been set for the concrete plug, and an initial porosity of 0.01 has been set for both the granite and the heaters (Table 2).

For the bentonite, the initial porosity has been set to 0.42 and the solid phase density has been set as 2.77 g/cm^3. Therefore, the initial dry density of the bentonite is approximately 1.61 g/cm^3. No double porosity has been considered for this model. The initial suction of the bentonite has been set to -135 MPa. Its initial relative humidity is 34%. Its initial degree of saturation is 65%.

Table 2. Initial conditions.

Material	Bentonite	Rock (granite)	Concrete plug	Heaters
Initial temperature (ºC)	12	12	12	12
Initial stress (MPa)	-0.1	-28	-0.1	-0.1
Initial pore water pressure (MPa)	-135	0.1 ─ 0.9	0	-20
Initial porosity	0.42	0.01	0.1	0.01
Solid phase density (g/cm^3)	2.77	2.75	2.6	8.93
Initial dry density (g/cm^3)	1.61	2.72	2.34	8.84
Initial relative humidity (%)	34	100	100	86
Initial degree of saturation (%)	65	100	80	81

2.3. Constitutive equations and material parameters

As mentioned above, four different materials have been modelled: the host rock (granite), the canisters (or heaters), the bentonite and the concrete plug. Table 3 shows a comparison of some relevant thermal and hydraulic parameters for all materials in the model. Table 4 in Appendix I shows all material parameters used for the granite, the concrete plug and the canister in Code_Bright.

Regarding the hydraulic and thermal constitutive equations, for the retention curve, the Van Genuchten model has been used:

$$S_e = \frac{S_l - S_{rl}}{S_{ls} - S_{rl}} = \left(1 + \left(\frac{P_g - P_l}{P}\right)^{\frac{1}{1-\lambda}}\right)^{-\lambda} \qquad \text{where} \qquad P = P_o \frac{\sigma}{\sigma_o}$$

Figure 6 shows the graphs corresponding to the retention curves used for bentonite and granite. Tables 4 and 5 include the parameters used in Code_Bright corresponding to these curves.

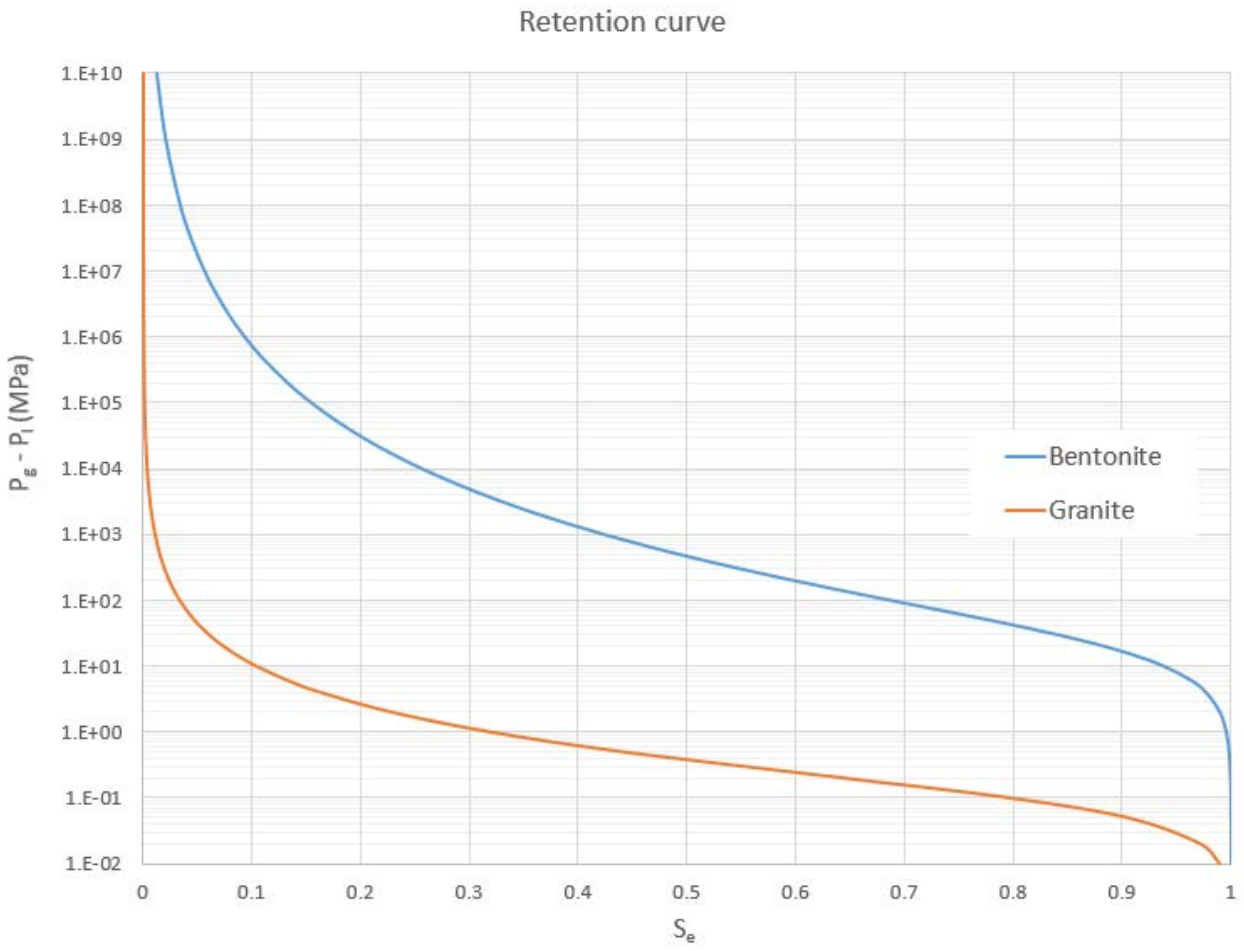

Figure 6. Retention curves for bentonite and granite

For the granite, the consistent form of relative permeability with van Genuchten model is used:

$$k_{rl} = \sqrt{S_e}\left(1 - \left(1 - S_e^{1/\lambda}\right)^{\lambda}\right)^2$$

Figure 7 shows the relative permeability of the granite.

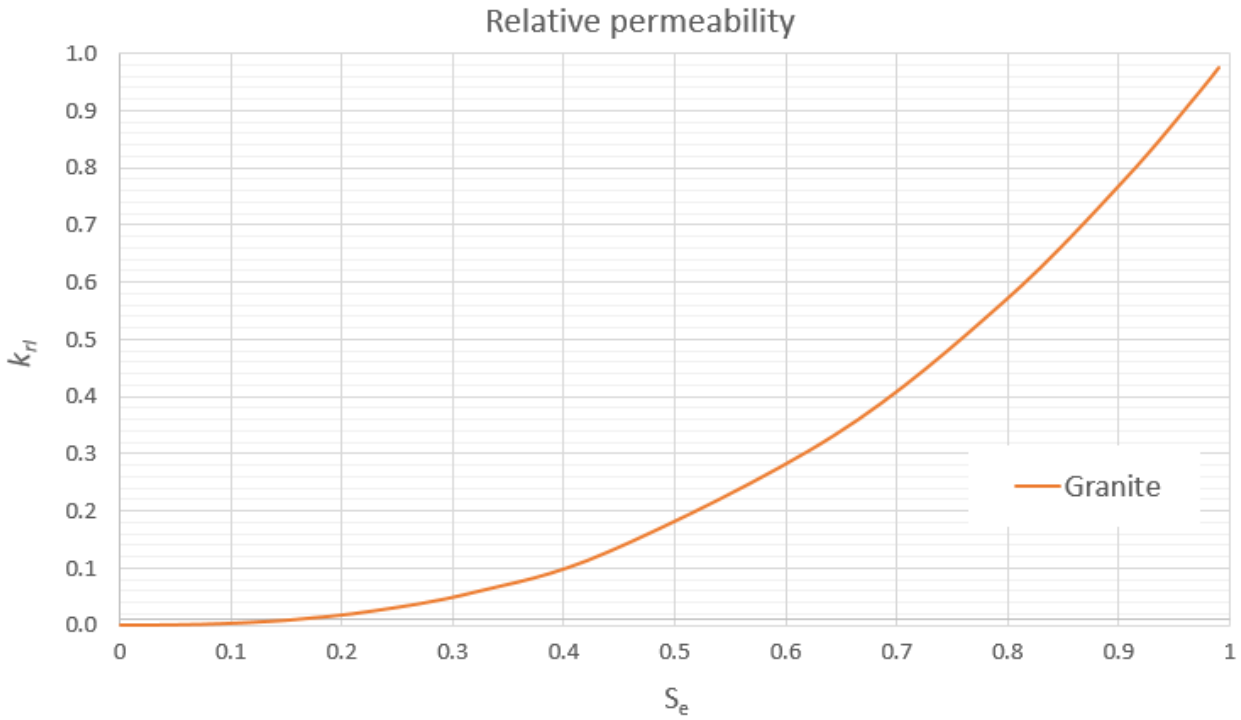

Figure 7. Relative permeability of the granite

For the liquid flow, Darcy's law has been used: $\mathbf{q}_\alpha = -\frac{\mathbf{k}k_{r\alpha}}{\mu_\alpha}\left(\nabla P_\alpha - \rho_\alpha \mathbf{g}\right)$

Where viscosity, density and relative permeability are defined in other laws and where, for a continuum medium (Kozeny's model), the intrinsic permeability **k** (Figure 8) is defined by:

$$\mathbf{k} = \mathbf{k}_o \frac{\varphi^3}{(1-\varphi)^2}\frac{(1-\varphi_o)^2}{\varphi_o{}^3}$$

where: φ_o : reference porosity

$\mathbf{k}_o$: intrinsic permeability for matrix φ_o

To compute the conductive heat flux, the thermal conductivity λ is used in Fourier's law:

$$\mathbf{i}_c = -\lambda \nabla T$$

In this case, the thermal conductivity depends on porosity by a geometric weighted mean:

$$\lambda_{dry} = \lambda_{solid}^{(1-\phi)}\lambda_{gas}^{\phi} \qquad \lambda_{sat} = \lambda_{solid}^{(1-\phi)}\lambda_{liq}^{\phi}$$

$$\lambda_{solid} = (\lambda_{solid})_o + a_1 T + a_2 T^2 + a_3 T^3$$

Where λ_{dry} is the thermal conductivity of the dry porous medium and λ_{sat} is the thermal conductivity of the water saturated porous medium.

Regarding the mechanical behaviour of the granite, a linear expansion law induced by temperature changes has been used:

$\Delta\varepsilon_v = 3\alpha_s \Delta T$ ($\Delta\varepsilon_v > 0$, extension; $\Delta\varepsilon_v < 0$, compression)

Moreover, a high elastic modulus 100 times bigger than normal has been set for the granite in the first interval (excavation) for the numerical convergence sake, but the normal value has been set in the rest of the intervals. The canister has been modelled as a dense, rigid, impermeable (very low permeability) and very conductive material.

Regarding the liquid phase properties, the water density has been modelled according to the following exponential variation law: $\rho_l = \rho_{l0} \exp(\beta(P_l - P_{lo}) + \alpha T + \gamma \omega_l^h)$

where:

Reference density	ρ_{lo}	1002.6	kg m^{-3}
Compressibility	β	4.5×10^{-4}	MPa^{-1}
Volumetric thermal expansion coefficient for water	α	-3.4×10^{-4}	C^{-1}
Solute variation	γ	0.6923	
Reference pressure	P_{lo}	0.1	MPa

And the liquid phase viscosity has been modelled according to the following law:

$$\mu_l = A\exp\left(\frac{B}{273.15+T}\right)$$

where:

Pre-exponential parameter	A	2.1×10^{-12}	MPa s
Exponential parameter	B	1808.5	K

The intrinsic permeability for the bentonite is considered 3E-21 m^2 for a reference porosity of 0.42 and is considered isotropic. The initial hydraulic conductivity would then be approximately 2.32E-14 m/s for the initial conditions (porosity of 0.42, temperature of 12 ºC and pressure of -135 MPa). Note that the intrinsic permeability changes with the porosity of the bentonite (Figure 8).

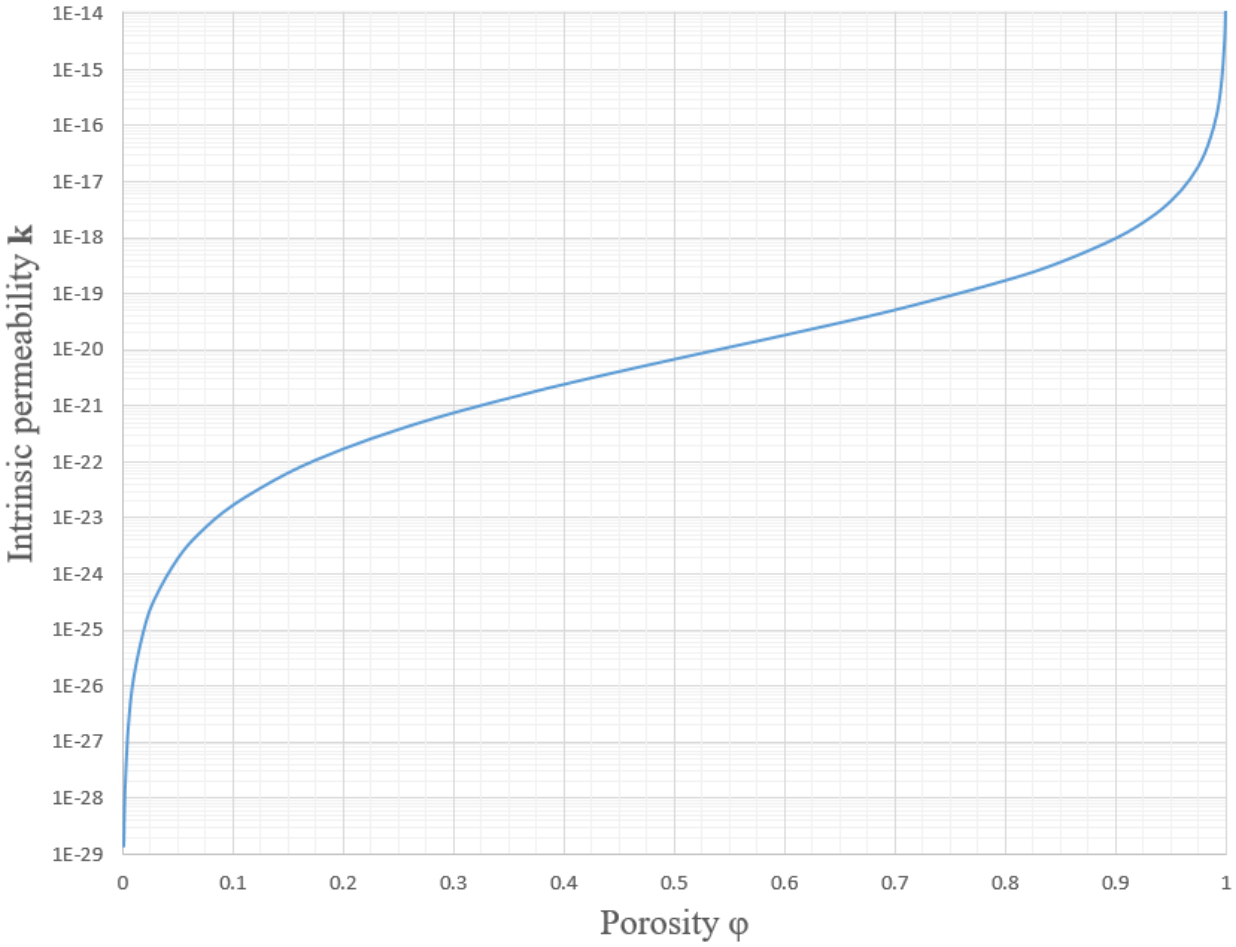

Figure 8. Change of the intrinsic permeability of the bentonite with the porosity.

Regarding the thermal conductivity, 4 W m^{-1} K^{-1} has been assigned for the granite and 2 W m^{-1} K^{-1} for the concrete plug. In the case of the heaters a high thermal conductivity of 390 W m^{-1} K^{-1} has been assign to make sure that the heat is homogeneously distributed throughout the heater. On the other side, different values have been assigned for the bentonite depending on its degree of saturation, according to the following empirical correlation:

$$\lambda = \frac{A_1 - A_2}{1 + e^{\left[{(Sr - Sr^*)}/{b}\right]}} + A_2$$

Where A_1 = 1.4 W m^{-1} K^{-1}, A_2 = 0.6 W m^{-1} K^{-1}, b = -0.12 and Sr^* = 0.6.

According to the equation and parameters mentioned above, Figure 9 shows the change in thermal conductivity of the bentonite with the liquid saturation degree.

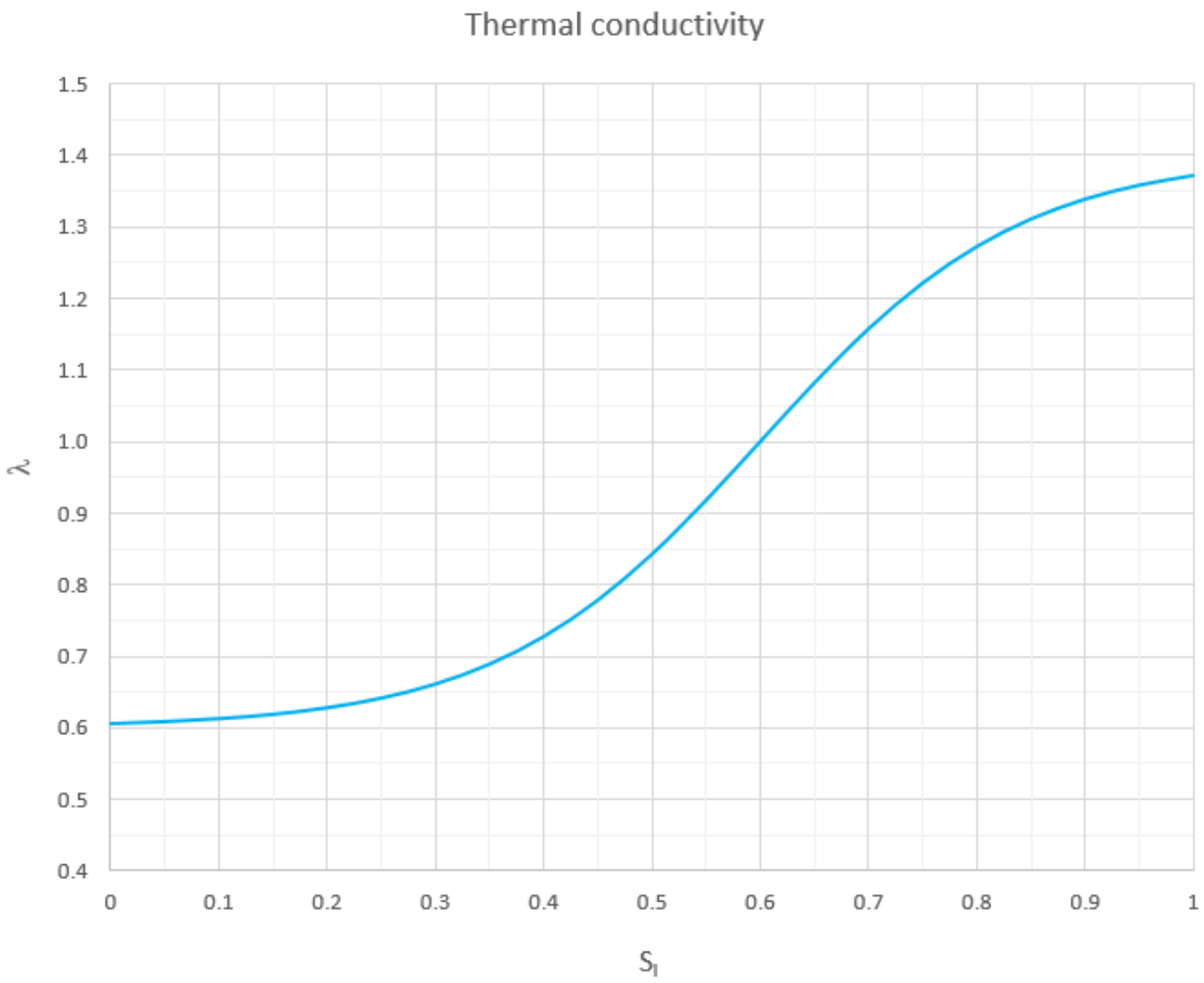

Figure 9. Thermal conductivity of the bentonite

Regarding the bentonite, Tables 5 and 6 in Appendix I show the constitutive laws used in the model and the properties corresponding to the FEBEX bentonite considered with single porosity. We consider that FEBEX bentonite can be represented with the Barcelona Basic Model or BBM (Alonso et al., 1990), van Genuchten model (van Genuchten, 1978 and 1980), Darcy's law, power relative permeability (Brooks and Corey, 1964) and the aforementioned correlation for thermal conductivity. The parameters are divided in hydraulic and mechanical parameters, which correspond to the Code_Bright materials input window (more information about these parameters in Code_Bright User's Guide).

Furthermore, a virtual swelling pressure test has been performed to determine the swelling pressure of the bentonite from initial conditions, obtaining a value of 5.7 MPa.

The different sets of parameters used to represent the properties of bentonite and granite are taken from the calibration work of different researchers (Gens et al., 2009; Villar, 2002; Ortuño et al., 2005; Frieg & Vomvoris, 1994). Note that in this model we use the standard van Genuchten for the retention curve instead of the modified version proposed in Gens et al. (2009).

Regarding the hydraulic and thermal parameters of the bentonite (Table 4 in Appendix I), the same constitutive laws as for the other materials have been used. Besides that, for the relative permeability of the liquid phase, a generalized power formulation has been used:

$$k_{rl} = AS_e^{\lambda}$$

Figure 10 shows the relative permeability corresponding to the bentonite.

Table 3. Thermal and hydraulic parameters.

Material	Bentonite	Rock (granite)	Concrete plug	Heaters
Initial intrinsic permeability (m^2)	3e-21*	8e-18	1e-18	1e-27
Initial hydraulic conductivity (m/s)	2.32e-14*	8e-11	1e-11	1e-20
Thermal conductivity dry (W m^{-1} K^{-1})	0.6	4	2	390
Thermal conductivity saturated (W m^{-1} K^{-1})	1.4	4	2	390
Swelling pressure (MPa)	5.7			

* Intrinsic permeability and hydraulic conductivity corresponding to a bentonite porosity of 0.42. Note that both the intrinsic permeability and the intrinsic permeability of the bentonite change with porosity (Figure 8).

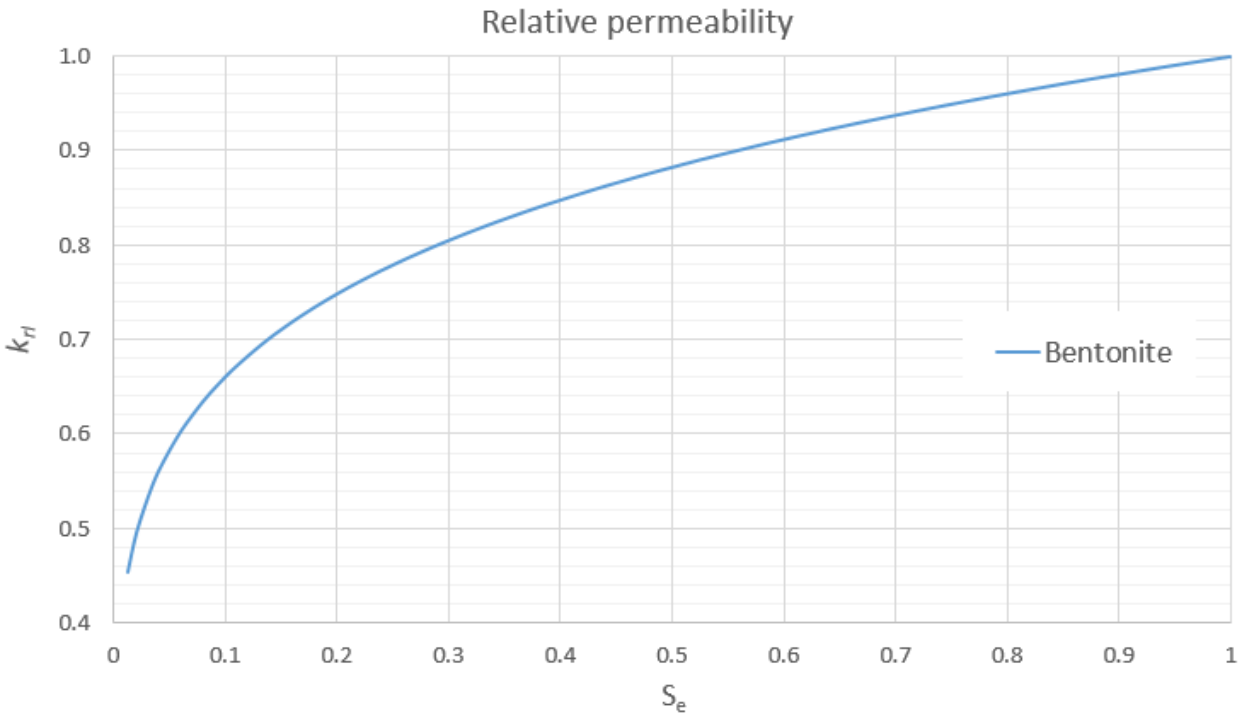

Figure 10. Relative permeability of the bentonite

For the diffusive fluxes of vapour, Fick's law for molecular diffusion has been used:

$$\mathbf{i}_{\alpha}^{i} = -\left(\tau\phi\rho_{\alpha}S_{\alpha}D_{\alpha}^{i}\mathbf{I}\right)\nabla\omega_{\alpha}^{i}$$

Where ϕ is porosity, ρ_{α} is density, S_{α} is degree of saturation, ω is mass fraction and $D_{\alpha}{}^{i}$ is the diffusion coefficient of species *i* in phase α in m^2/s.

The non-advective flux of a species in a phase is composed by molecular diffusion and mechanical dispersion (dispersion is defined in another set of parameters).

Molecular diffusion of vapour or air in the gas phase:

$$D_{\alpha}^{i} = D\left(\frac{\left(273.15+T\right)^{n}}{P_{g}}\right)$$

Where P_g is the gas pressure in Pa, and D and n are parameters. Tortuosity is defined as a constant value in this case:

$$\tau = \text{constant}=\tau_{0}$$

3. Sensitivity analysis performed

Three sensitivity analysis were performed including the following bentonite parameters: intrinsic permeability, initial porosity and thermal conductivity.

3.1. Sensitivity to bentonite intrinsic permeability

Three different models have been developed using three different values for the bentonite intrinsic permeability and a sensitivity analysis have been performed over different variables.

For instance, Figure 11 shows the effect of intrinsic permeability on the degree of saturation at the final dismantling (6758 days). As it can be observed, slight changes in the intrinsic permeability affect significantly the degree of saturation of the bentonite barrier at the final dismantling. In this figure, we can also see the comparison with real measurements. Moreover, the intrinsic permeability of the bentonite is somewhat uncertain, especially due to the existence of gaps between bentonite blocks and between the blocks and the host rock of the heater. Therefore, in situ intrinsic permeability is expected to have a higher value than that obtained in the laboratory. In any case, note that intrinsic permeability varies with porosity and that the given values are not constant, but referenced to a porosity of 0.4. This analysis have been used to estimate an initial intrinsic permeability of 3e-21 for a reference porosity of 0.42, which is also the initial porosity, considering the aforementioned gaps effect.

In addition, in Figures 12 and 13 it can be observed that the intrinsic permeability has not a significant influence on the dry density or the water content. However, the measurements are quite far for the model results, which motivated the following sensitivity analyses.

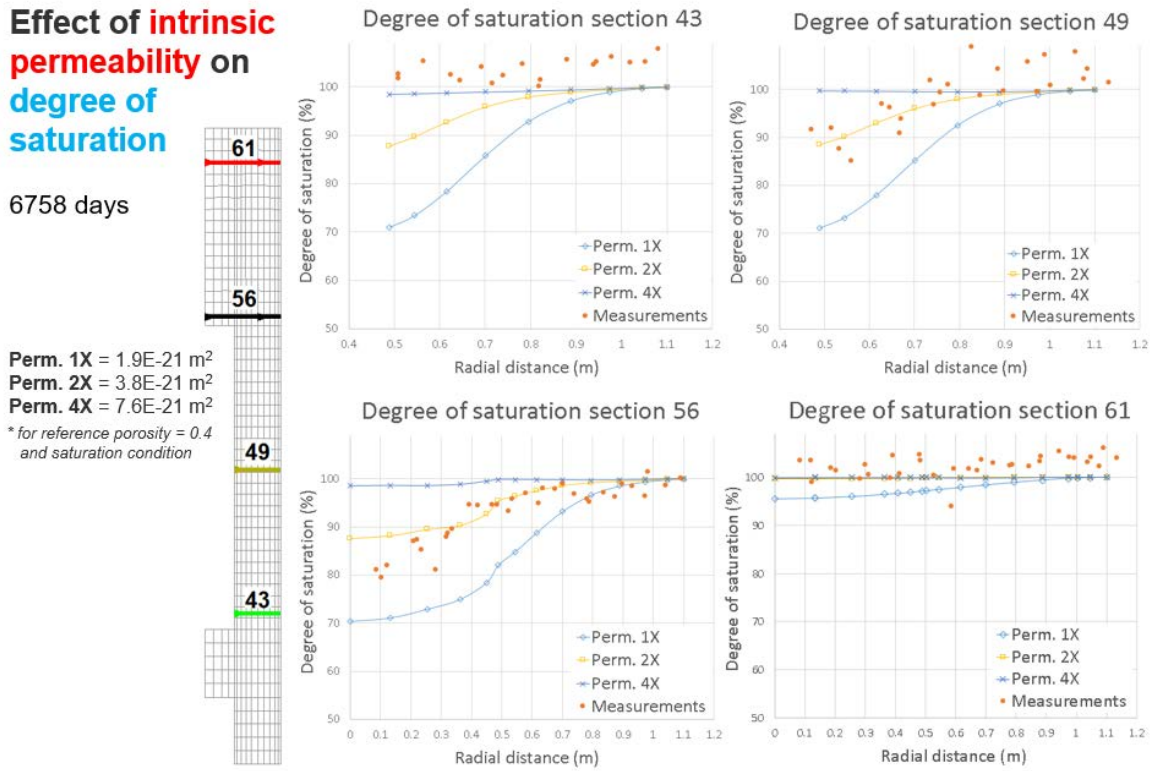

Figure 11. Effect of the bentonite intrinsic permeability on the degree of saturation.

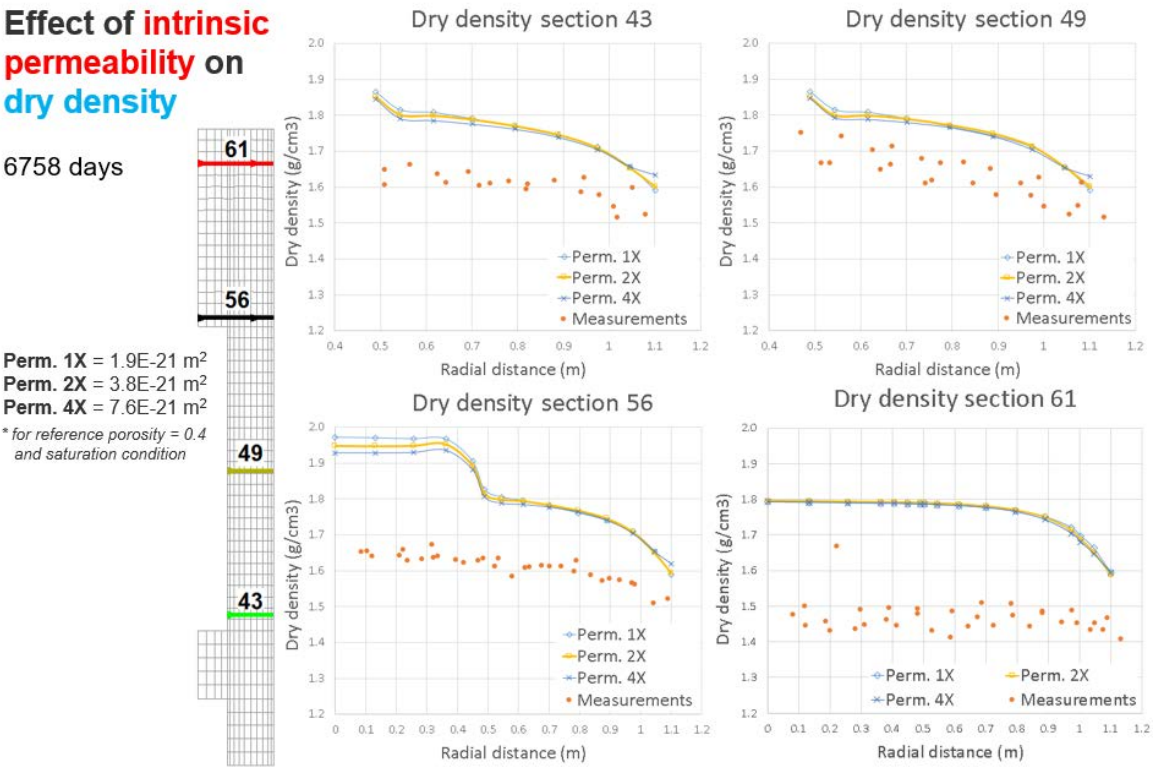

Figure 12. Effect of the bentonite intrinsic permeability on the dry density.

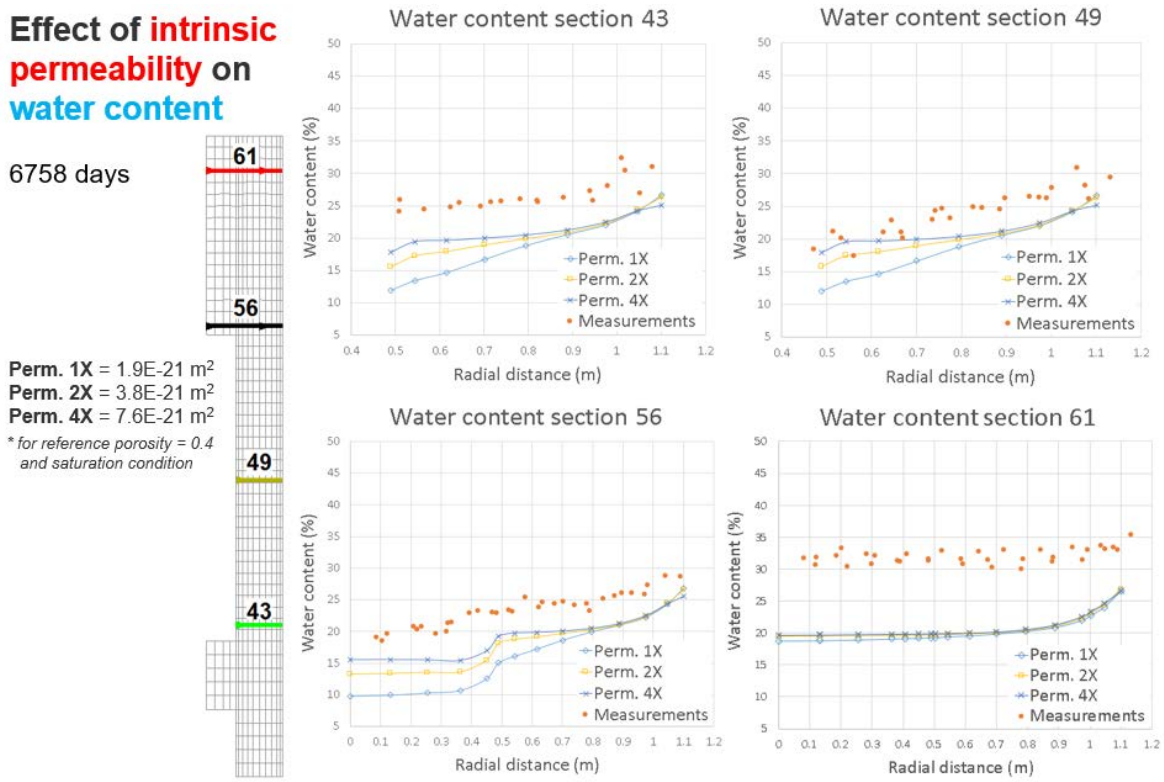

Figure 13. Effect of the bentonite intrinsic permeability on the water content.

3.2. Sensitivity to bentonite initial porosity

In the last epigraph, we mentioned the possible effect of the gaps on the intrinsic permeability. For the same reason, the initial dry density of a brick of bentonite may not be representative of the whole bentonite barrier. Therefore, we have performed an analysis of the effect of the initial porosity considering both estimated values for the brick and the whole barrier.

In Figures 14 and 15, it can be observed that the value of the initial porosity (or, as a consequence, the value of the initial dry density) significantly affects the final values of the dry density and water content for the final state of the bentonite barrier. This means that an initial porosity of 0.42, which gives the estimated value of dry density for the whole bentonite barrier, could be more representative of the initial state of the barrier, so that value for the initial porosity has been taken for the final model. It should also be noted that section 61 is significantly off the measurements, probably due to a big gap between the bentonite barrier end the end of the tunnel excavation. Moreover, in Figure 16 it can be observed that the initial porosity has also an effect on the final degree of saturation in the same direction as an increase of the permeability.

In addition, it has been tested the effect of these changes on other variables in the model and it can be concluded, in general, that they do not have a significant effect on different variables such as temperature. Although they affect slightly the stresses, it is difficult to state whether these effects take us closer or further from the measurements, due to their uncertainty, being different depending on the section analysed. Finally, there is an effect on the heating power, but it will be analysed in the following section.

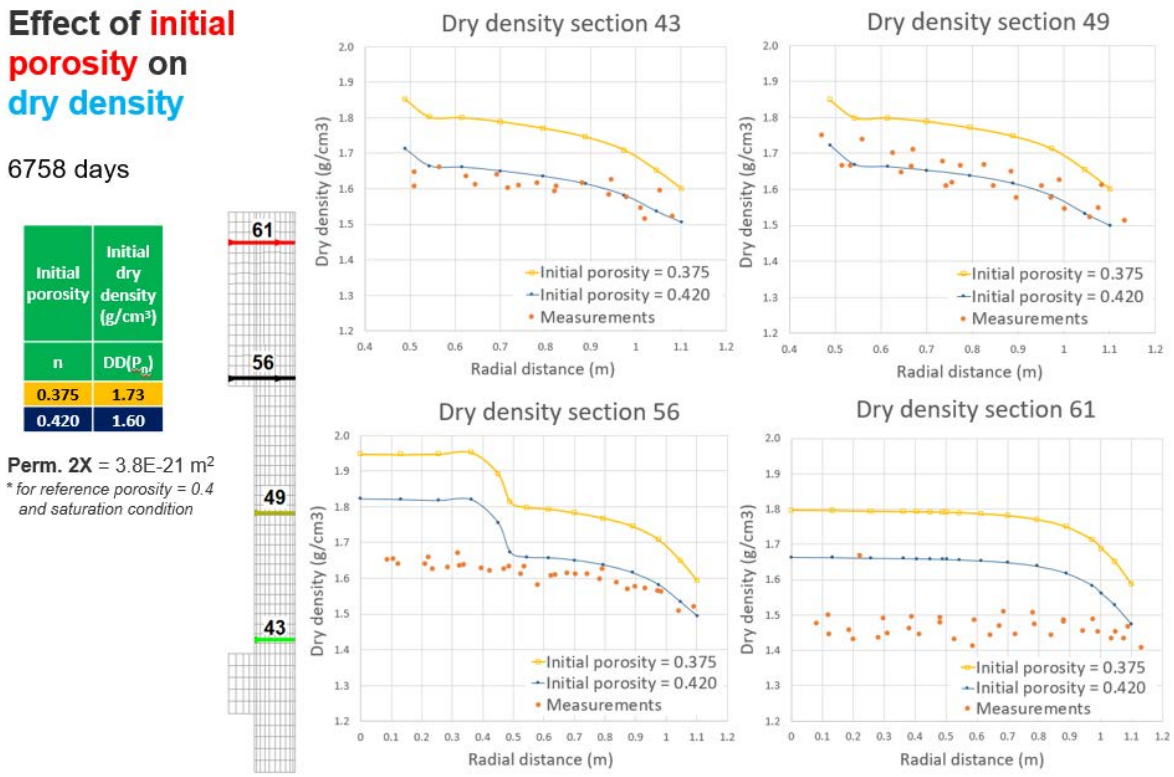

Figure 14. Effect of the bentonite initial porosity on the dry density.

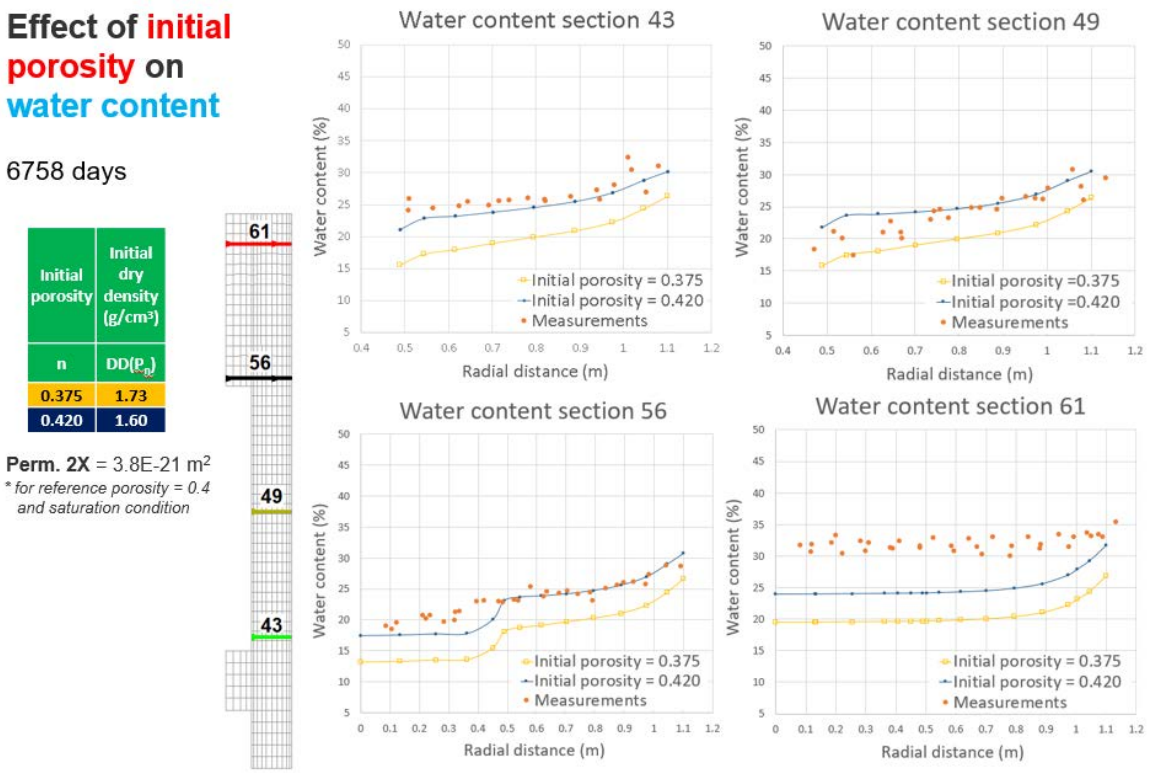

Figure 15. Effect of the bentonite initial porosity on the water content.

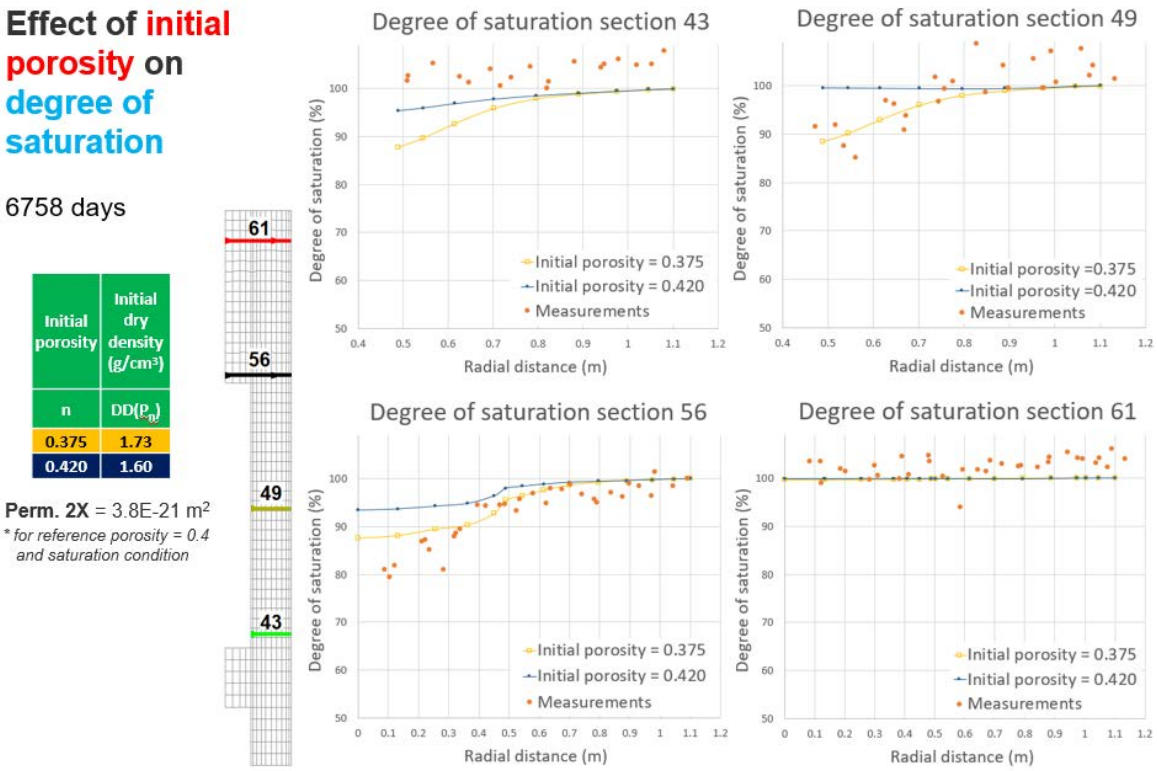

Figure 16. Effect of the bentonite initial porosity on the degree of saturation.

3.3. Sensitivity to bentonite thermal conductivity

As mentioned in the last section, the sensitivity analyses performed so far have also an influence on the heating power, as shown in Figure 17, mainly because heat conductivity and liquid advection increase with higher permeability values. Anyway, the results obtained underestimate the in situ measurements. For that reason, we have performed a final sensitivity analysis of the bentonite thermal conductivity.

Figure 18 shows the different functions and values used for the sensitivity analysis including the s-shaped function corresponding to this final report (Figure 9). It should be noted that cases R27 and R29 from Figure 18 give similar results although they use different functions, since most of the bentonite barrier has a degree of saturation higher than 65% from the beginning, from which point both functions are similar.

Finally, in Figure 19 it can be observed that the heating power is much closer to the measurements using high thermal conductivity (either case R27 or case R29) than the results obtained from the "base case" (permeability 1X and initial porosity of 0.375) or after the corrections from the previous sensitivity analysis (permeability 2X and initial porosity of 0.42). Therefore, the s-shaped function from Figure 9 has been taken for the final model.

Effect of intrinsic permeability and initial porosity on heating power

- Heat conductivity increases.
- Liquid advection increases.

Initial porosity	Initial dry density (g/cm³)
n	DD(P_{00})
0.375	1.73
0.420	1.60

Perm. 1X = 1.9E-21 m²
Perm. 2X = 3.8E-21 m²
** for reference porosity = 0.4 and saturation condition*

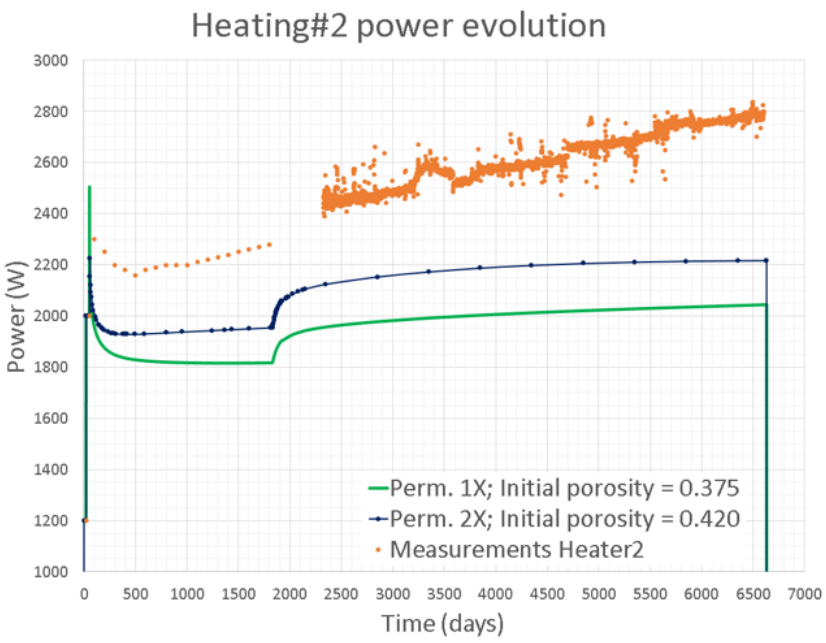

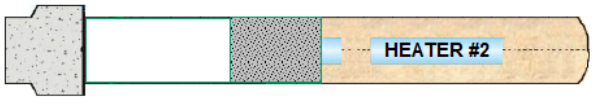

Figure 17. Effect of intrinsic permeability and initial porosity on the heating power.

Effect of thermal conductivity on heating power

$$\lambda = \lambda_{sat}^{S_l} \lambda_{dry}^{(1-S_l)}$$

λ_{dry}	W m^{-1} K^{-1}	0.47
λ_{sat}	W m^{-1} K^{-1}	1.15

λ_{dry}	W m^{-1} K^{-1}	0.6
λ_{sat}	W m^{-1} K^{-1}	1.4

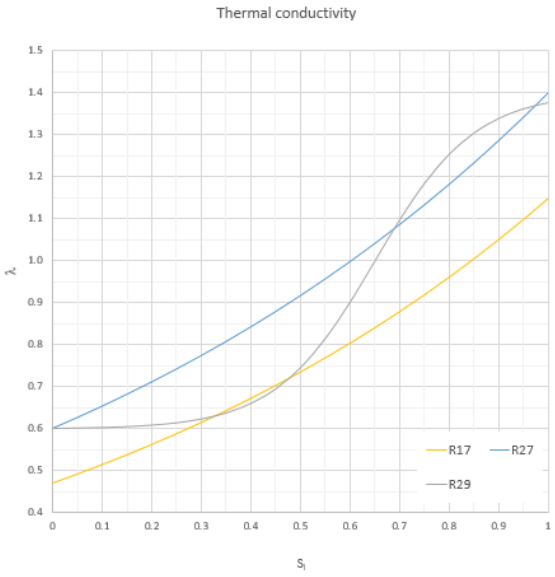

parameter	bentonite S-2	FEBEX bentonite
A_1	0.39 ± 0.08	0.57± 0.02
A_2	1.34 ± 0.06	1.28 ± 0.03
x_0	0.54 ± 0.03	0.65 ± 0.01
d_x	0.15 ± 0.03	0.10 ± 0.02

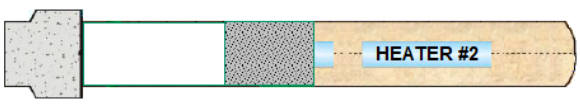

Figure 18. Thermal conductivity different functions used in for the sensitivity analysis.

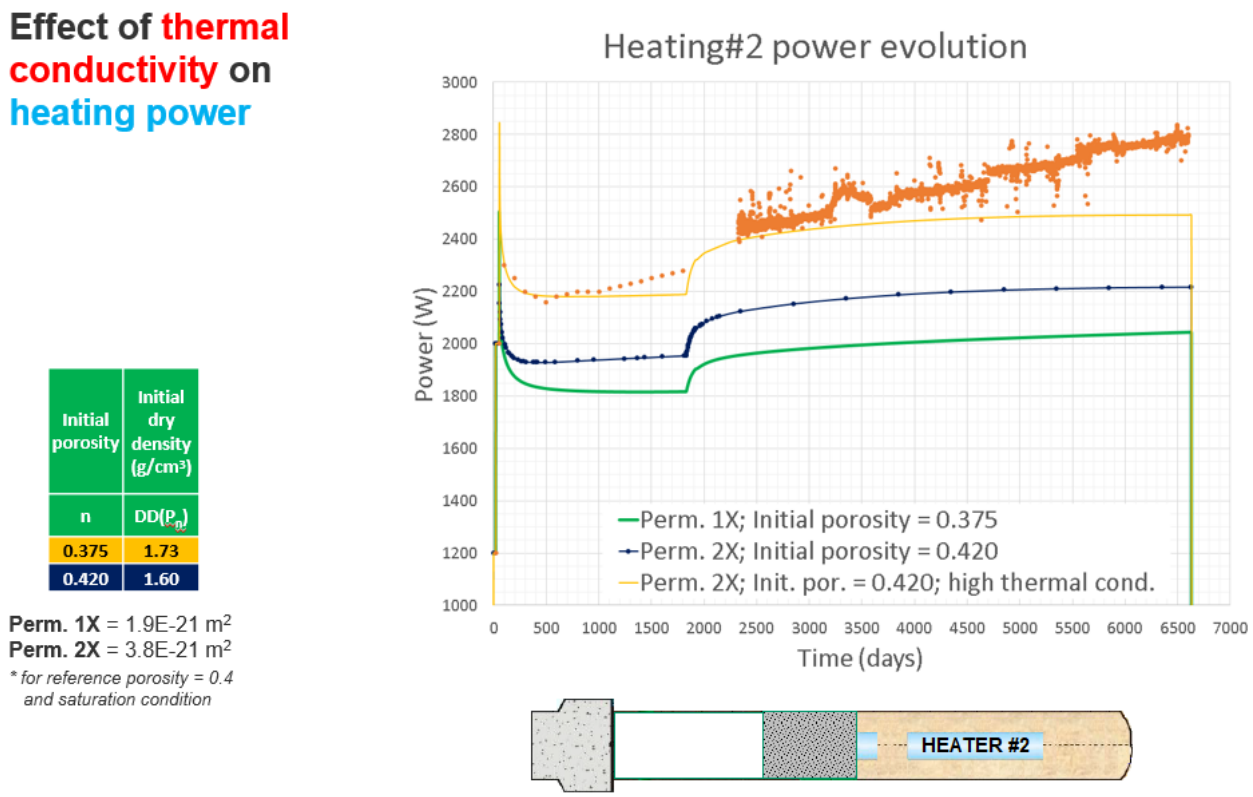

Figure 19. Effect of thermal conductivity and initial porosity on the heating power.

4. References

Alonso E, Gens A, Josa A. A constitutive model for partially saturated soils. Geotech. 1990;40(3):405-30.

Alonso E, Alcoverro J. The FEBEX test as a benchmark case for THM modelling: historical perspective and lessons learnt. In: Alonso E, Ledesma A, editors. Advances in understanding engineered clay barriers, London: Taylor & Francis; 2005, p. 3-19.

Bendito E, Pintado X. Monitoring of swelling pressure in bentonite. Environmental Geotechnics 2016, 3:5, 334-345.

Brooks RH, Corey AT. Hydraulic Properties of Porous Media. Hydrologic Paper 3, Colorado State University, Fort Collins, USA, 1964.

Code_Bright User's Guide. Civil and Environmental Engineering Department, Technical University of Catalonia, Spain, 2018 (available at deca.upc.edu/en/projects/code_bright).

Frieg B, Vomvoris S. Investigation of hydraulic parameters in the saturated and unsaturated zone of the ventilation drift, Technical Report 93-10. Baden: Nagra, 1994.

Gens A, Garcia-Molina AJ, Olivella S, Alonso E, Huertas F. Analysis of a full scale in situ test simulating repository conditions. Int J Numer Anal Methods Geomech. 1998;22(7):515-48.

Gens A, Sanchez M, Guimaraes LDN, Alonso E, Lloret A, Olivella S et al. A full-scale in situ heating test for high-level nuclear waste disposal: observations, analysis and interpretation. Geotech. 2009;59(4):377-99. doi: 10.1680/geot.2009.59.4.377

Huertas F, Farina P, Farias J, Garcıa-Siñeriz JL, Villar MV, Fernandez AM, et al. Full-scale engineered barrier experiment. ENRESA, Madrid. Updated final report, technical publication 05-0/2006.

Olivella S, Carrera J, Gens A, Alonso, E. Nonisothermal multiphase flow of brine and gas through saline media. Transport in Porous Media, 1994:15(3):271–293. doi:10.1007/BF00613282

Olivella S, Gens A, Carrera J, Alonso E. Numerical formulation for a simulator 'CODE_BRIGHT' for the coupled analysis of saline media. Engng Comput. 1996;13(7):87-112.

Ortuño F, Carretero G, Martinez-Landa L, Carrera J. Hydraulic characterisation of the FEBEX granite: test performance and field interpretation. In Advances in understanding engineered clay barriers (eds E. E. Alonso and A. Ledesma), pp. 133-141. London: Taylor & Francis, 2005.

Rodriguez-Dono A, Olivella S and Mokni N. Assessment of a high-level spent nuclear fuel disposal model. Environmental Geotechnics 0 0:0, 1-17, https://doi.org/10.1680/jenge.18.00017

Sanchez M & Gens A. FEBEX project: Final report on thermo-hydro-mechanical modelling, Technical Publication 05-2/2006. Madrid: Enresa.

Sanchez M, Gens A, Guimaraes L. Thermal–hydraulic–mechanical (THM) behaviour of a large-scale in situ heating experiment during cooling and dismantling. Canadian Geotechnical Journal, 2012, 49(10): 1169-1195, https://doi.org/10.1139/t2012-076

Tadikonda VB. Analytical model for 1-D contaminant diffusion through clay barriers. Environmental Geotechnics 2014, 1:4, 210-221.

Toprak E, Olivella S, Pintado X. Modelling Engineered Barriers for Spent Nuclear Fuel Repository using a Double Structure Approach for Pellet based Components. Environmental Geotechnics 2018, 1-70.

van Genuchten R. Calculating the unsaturated hydraulic permeability conductivity with a new closed-form analytical model. Water Resources Research, 1978:37(11): 21–28.

van Genuchten R. A closed-form equation for predicting the hydraulic conductivity of unsaturated soils. Soil Science Society American Journal, 1980, 44: 892-898.

Villar MV. Thermo-hydro-mechanical characterisation of a bentonite from Cabo de Gata: A study applied to the use of bentonite as sealing material in high-level radioactive waste repositories, Technical Publication 01/2002. Madrid: Enresa.

Villar MV, Iglesias RJ, Garcia-Siñeriz JL. A Heterogeneous Bentonite Barrier after 18 Years Operation: Final Physical State of the Bentonite Barrier of the Febex in Situ Test. Environmental Geotechnics 2018, 1-45.

Appendix I. Mechanical, hydraulic and thermal parameters used in Code_Bright

Table 4. Main material parameters for the granite, the concrete plug and the canister. See Code_Bright User's Guide for further details.

MECHANICAL DATA			
	Granite	**Concrete plug**	**Canister**
Linear elasticity (ITYCL=1)			
P1: E (MPa)	11697	30000	21000
P3: ν	0.3	0.3	0.3
HYDRAULIC AND THERMAL DATA			
Retention Curve (ITYCL=1)			
P1: P_o (MPa)	0.1	0.1	27
P3: λ	0.33	0.33	0.45
P5: S_{ls}	1	1	1
Intrinsic Permeability (ITYCL=1)			
P1: $(k_{11})_o$ (m^2)	8.e-18	1.e-18	1.e-27
P2: $(k_{22})_o$ (m^2)	8.e-18	1.e-18	1.e-27
P3: $(k_{33})_o$ (m^2)	8.e-18	1.e-18	1.e-27
Conductive flux of heat 1 (ITYCL=1)			
P1: λ_{dry} (W m^{-1} K^{-1})	4	2	390
P2: λ_{sat} (W m^{-1} K^{-1})	4	2	390
PHASE PROPERTIES			
Solid phase (ITYCL=1)			
P1: C_s (J kg^{-1} K^{-1})	793	1000	390
P2: ρ_s (kg m^{-3})	2750	2600	8930
P3: α_s (C^{-1})	7.8e-6	0	1.2e-5

Table 5. Physical, hydraulic and thermal parameters for bentonite.
See Code_Bright User's Guide for further details.

Retention curve (ITYCL=1)		
P1: P_o (MPa)	20	Van Genuchten model:
P2: σ_o (N m^{-1})	0.072	$S_e = \frac{S_l - S_{rl}}{S_{ls} - S_{rl}} = \left[1 + \left(\frac{P_g - P_l}{P}\right)^{\frac{1}{1-\lambda}}\right]^{-\lambda}$ $\quad P = P_o \frac{\sigma}{\sigma_o}$
P3: λ	0.18	
P4: S_{rl}	0.01	
P5: S_{ls}	1	
Intrinsic permeability (ITYCL=1)		
P1: $(k_{11})_o$ (m^2)	3e-21	Darcy's law: $\mathbf{q}_l = -\frac{\mathbf{k} k_{rl}}{\mu_l}(\nabla P_l - \rho_l \mathbf{g})$
P2: $(k_{22})_o$ (m^2)	3e-21	
P3: $(k_{33})_o$ (m^2)	3e-21	Kozeny's model: $\mathbf{k} = \mathbf{k}_o \frac{\phi^3}{(1-\phi)^2}\frac{(1-\phi_o)^2}{\phi_o{}^3}$
P4: ϕ_o	0.42	
Liquid phase relative permeability (ITYCL=6)		
P2: A	1	$k_{rl} = A S_e{}^{\lambda}$
P3: λ	3	
P4: S_{rl}	0.01	
P5: S_{ls}	1	
Diffusive flux of vapour (ITYCL=1)		
P1: D (m^2 s^{-1} K^{-n} Pa)	5.9e-6	Fick's law for molecular diffusion:
P2: n	2.3	$\mathbf{i}_g^w = -(\tau\phi\rho_g S_g D_m^w \mathbf{I})\nabla\omega_g^w D_m^{vapor} = D\left[\frac{(273.15+T)^n}{P_g}\right]$
P3: τ_o	0.8	$\tau = \text{constant} = \tau_o$
Conductive flux of heat 1 (ITYCL=1)		
ITYCL	1	Fourier's law: $\mathbf{i}_c = -\lambda\nabla T$
P1: λ_{dry} (W m^{-1} K^{-1})	0.6	$\lambda = \lambda_{sat}^{S_l}\lambda_{dry}^{(1-S_l)}$
P2: λ_{sat} (W m^{-1} K^{-1})	1.4	
Conductive flux of heat 2 (ITYCL=7)		
P1: b	-0.12	$\lambda = \frac{A_1 - A_2}{1 + e^{\left[(Sr - Sr^*)/b\right]}} + A_2$
P2: Sr^*	0.6	
Solid phase properties (ITYCL=1)		
P1: C_s (J kg^{-1} K^{-1})	1000	
P2: ρ_s (kg m^{-3})	2770	
P3: α_s (C^{-1})	7.8e-6	

Table 6. Mechanical parameters for bentonite. Thermo-elasto-plastic (TEP) model. See Code_Bright User's Guide for further details.

Elastic parameters (ITYCL=1)	
P1: k_{io}	0.05
P2: k_{so}	0.25
P3: K_{min} (MPa)	10
P5: v	0.4
P8: α_i	-0.003
P9: α_{sp}	-0.161
P10: p_{ref} (MPa)	0.01
Thermal and other parameters (ITYCL=1)	
P1: α_o	1.5e-4
P5: T_{ref} (C)	20
Plastic parameters 1 (ITYCL=1)	
P1: $\lambda(0)$	0.15
P2: r	0.925
P3: β (MPa^{-1})	0.05
P4: ρ (C^{-1})	0.2
P5: k	0.1
P6: p_{so} (MPa)	0.1
Plastic parameters 2 (ITYCL=1)	
P1: p^c (MPa)	0.5
P2: M	1
P3: α	0.53
P4: e_o	0.6
P5: p_o^* (MPa)	12
Parameters shape yield surf. (ITYCL=3)	
Parameters shape plastic pot. (ITYCL=3)	
Integration control parameters (ITYCL=1)	
P1: *Tole1*	1e-7
P2: *Tole2*	1e-4
P3: *Tole3*	1e-3
P4: μ	1
P5: *Index*	1
P7: *Itermaxs*	20

$$d\varepsilon_v^e = \frac{k_i(s)}{1+e}\frac{dp'}{p'} + \frac{k_s(p',s)}{1+e}\frac{ds}{s+0.1} + (\alpha_o)dT$$

where:

$$k_i(s) = k_{io}\left(1+\alpha_i s\right)$$

$$k_s(p',s) = k_{so}\left(1+\alpha_{sp}\ln p'/p_{ref}\right)$$

$$p_o = p^c\left(\frac{p_o^*(T)}{p^c}\right)^{\frac{\lambda(o)-kio}{\lambda(s)-kio}}$$

$$p_o^*(T) = p_o^*$$

$$\lambda(s) = \lambda(o)\left[(1-r)\exp\left(-\beta s\right)+r\right]$$

$$p_s = p_{so} + k\,s\exp(-\rho\Delta T)$$

$$\Delta T = T - T_{ref}$$

$$g_y(\theta)=1$$

$$g_p(\theta)=1$$

Appendix II. EBS Task Force requested tables.

Rock

Initial conditions of the rock at the start of the analysis (1)

Initial temperature at tunnel axis level (C)	Initial stresses at tunnel axis level (MPa)	Initial pore water pressure at tunnel axis level (MPa)
12	-28	-1*

*At the tunnel boundary, there is an initial pore water pressure of -1 MPa, simulating ventilation, but the far rock mass has an initial pore water pressure of 0.9 MPa (Figure 5).

Initial conditions of the rock at the start of the analysis (2)

Initial density (g/cm^3)	Initial porosity	Initial water content (%)
2.75	0.01	0.4

Main rock properties (1)

Initial thermal conductivity (W m^{-1} K^{-1})	Specific heat capacity (J kg^{-1} K^{-1})	Initial intrinsic permeability (m^2)	Initial hydraulic conductivity (m/s)
4	793	8e-18	8e-11

Main rock properties (2)

Linear thermal expansion coefficient (K^{-1})	Young's modulus (MPa)	Poisson's ratio
7.8e-6	11697	0.3

Main rock properties: retention curve (3)

Equation used	P_o (MPa)	λ
$S_e = \left(1+\left(\frac{P_g - P_l}{P_o}\right)^{\frac{1}{1-\lambda}}\right)^{-\lambda}$	0.1	0.33

Main rock properties: relative permeability (4)

Equation used	λ
$k_{rl} = \sqrt{S_e}\left(1-\left(1-S_e^{1/\lambda}\right)^{\lambda}\right)^2$	0.33

Bentonite

Initial conditions of the bentonite at installation (1)

Initial temperature (C)	Initial stresses (MPa)	Initial pore water pressure/suction (MPa)	Initial relative humidity (%)
12	-0.1	-135	34

Initial conditions of the bentonite at installation (2)

Initial dry density (g/cm^3)	Initial density of the solid phase (g/cm^3)	Initial porosity	Initial water content (%)	Initial degree of saturation (%)
1.61	2.77	0.42	16	65

Main bentonite properties (1)

Initial thermal conductivity ($W\ m^{-1}\ K^{-1}$)	Initial thermal conductivity dry bentonite ($W\ m^{-1}\ K^{-1}$)	Initial thermal conductivity saturated bentonite ($W\ m^{-1}\ K^{-1}$)	Initial specific heat capacity of the solid phase ($J\ kg^{-1}\ K^{-1}$)	Linear thermal expansion coefficient (K^{-1})
1.08	0.6	1.4	1000	7.8e-6

Main bentonite properties (2)

Initial intrinsic permeability (m^2)	Initial hydraulic conductivity (m/s)	Initial intrinsic permeability (saturated) (m^2)	Initial hydraulic conductivity (saturated) (m/s)	Swelling pressure under initial conditions (oedometric conditions) (MPa)
3e-21[*,+]	2.3e-14[*,+]	5.6e-21[*,x] 5.2e-20[*,°]	4.3e-14[*,x] 4e-13[*,°]	5.7

[*] Note that both intrinsic permeability and hydraulic conductivity change with porosity (Figure 8).

[+] At an initial relative permeability $k_{rl} = 0.925$.

[x] At a porosity = 0.48 (saturated conditions in FEBEX model).

[°] At a porosity = 0.7 (saturated conditions in oedometer).

Main bentonite properties: intrinsic permeability dependence on porosity (3)

Equation used	$(k_{11})_o$ (m^2)	$(k_{22})_o$ (m^2)	$(k_{33})_o$ (m^2)	φ_o
$\mathbf{k} = \mathbf{k}_o \frac{\varphi^3}{(1-\varphi)^2} \frac{(1-\varphi_o)^2}{\varphi_o^3}$	3E-21	3E-21	3E-21	0.42

Main bentonite properties: retention curve (4)

Equation used	P_o (MPa)	λ
$S_e = \left(1 + \left(\frac{P_g - P_l}{P_o}\right)^{\frac{1}{1-\lambda}}\right)^{-\lambda}$	20	0.18

Main bentonite properties: relative permeability (5)

Equation used	A	λ
$k_{rl} = AS_e^{\lambda}$	1	3

Main bentonite properties: thermal conductivity (6)

Equation used	A_1 (W m^{-1} K^{-1})	A_2 (W m^{-1} K^{-1})	b	Sr^*
$\lambda = \frac{A_1 - A_2}{1 + e^{\left[(Sr - Sr^*)/b\right]}} + A_2$	1.4	0.6	-0.12	0.6

Main bentonite properties: vapour transport (7)

Molecular diffusion coefficient of vapour in free air (m^2/s)	Tortuosity
2.61e-5*	0.8

* At 12ºC and 0.1 MPa